Title	Applicability and limitations of $G(r,E)$ analysis transformed from the inelastic neutron scattering data
Author(s)	Nakamura Mitsutaka, Kikuchi Tatsuya, Kawakita Yukinobu
Citation	Physica B; Condensed Matter,567,p.61-64
Text Version	Accepted Manuscript
URL	https://jopss.jaea.go.jp/search/servlet/search?5063096
DOI	https://doi.org/10.1016/j.physb.2019.01.002
Right	© 2019. This manuscript version is made available under the CC-BY-NC-ND 4.0 license http://creativecommons.org/licenses/by-nc-nd/4.0/

Applicability and limitations of $G(r, E)$ analysis transformed from the inelastic neutron scattering data

Mitsutaka Nakamura[*,a], Tatsuya Kikuchi[a,b], Yukinobu Kawakita[a]

[a] *Materials and Life Science Division, J-PARC Center, Japan Atomic Energy Agency, Tokai, Ibaraki 319-1195, Japan*
[b] *Sumitomo Rubber Industries, LTD., Kobe, Hyogo 651-0072, Japan*

Abstract

We have systematically investigated the dynamical structure factor in real-space $G(r, E)$ of polycrystalline Ni transformed from the inelastic neutron scattering data $S(Q, E)$. In particular, we have extensively explored the effects of different Q-E ranges of $S(Q, E)$ on the accuracy of $G(r, E)$. Our analyses have proven that atomic pair correlations at the first nearest neighbor distance can be reasonably evaluated by $G(r, E)$ transformed from the conventional $S(Q, E)$ where the covered Q-E range is not so wide.

Key words: Inelastic neutron scattering, Phonon dynamics, Real-space analysis

1. Introduction

Inelastic neutron scattering (INS) is a powerful tool used to investigate the dynamical structure factor $S(Q, E)$ of various materials. By deriving the Fourier transform of $S(Q, E)$ for the momentum transfer Q, we can obtain the dynamical structure factor in real-space $G(r, E)$. This procedure is not trivial, as $S(Q, E)$ needs to be defined to large values Q to yield a correct Fourier transform. Several attempts to convert $S(Q, E)$ into $G(r, E)$ have been made under special conditions, including large sample amounts and long measurement times. In addition to theoretical studies[1, 2], this problem has been addressed in experimental reports, such as those for amorphous boron [3], vitreous silica [4, 5], relaxor ferroelectric [6], and $FeSe_xTe_{1-x}$ [7]. The recent development of high-flux neutron beams enables a reduction in the required sample amount and measurement time for a $G(r, E)$ analysis. Egami *et al.* reported the real-space atomic correlation of Pb-free ferroelectrics[8] and liquid helium[9] by using the chopper spectrometer at the Spallation Neutron Source in Oak Ridge National Laboratory.

In Japan Proton Accelerator Research Complex (J-PARC), we have also independently developed the software used to deduce the dynamical structure factor in real-space from the inelastic and quasielastic neutron scattering data, recently publishing a $G(r, E)$ study of NaI[10], as well as a $P(r, t)$ study of liquid bismuth[11]. The special feature of our analysis is its utilization of information entropy. Our study of NaI[10] has shown that meaningful information on phonon dynamics close to the first nearest neighbor (NN) distance for NaI can be obtained using $G(r, E)$ with an incident energy E_i of 36.9 meV. Compared to the $S(Q, E)$ presented in previously published studies [3, 4, 5, 6, 7], the Q-E range covered by INS measurement with E_i = 36.9 meV was not as wide. Due to the difficulties in a Fourier transform, the experimental condition of E_i = 36.9 meV was considered as conventional for measurements addressing the Q-E space, but not appropriate for the investigation of r-E space. Our findings on NaI are important because they may inspire a new perspective in further research development, by utilizing a large amount of previously measured $S(Q, E)$ data.

This study was conducted to confirm the validity of our analysis method and focuses on the effect differing Q-E ranges of $S(Q, E)$ may have on the accuracy of $G(r, E)$. We have performed INS measurements of polycrystalline Ni, which is frequently used as a standard sample to investigate features of $G(r, E)$[2, 6, 7]. Further research utilizing our newly-developed $G(r, E)$ analytical method should be based on this study, as well as our previous works [10].

*Corresponding author. Tel: +81 29 284 3198
Email address: mitsutaka.nakamura@j-parc.jp (Mitsutaka Nakamura)

Condition	E_i [meV]	$2\theta_{max}$	Q_{max} [Å^{-1}]	Δr [Å]
110Ei-m1	110.6	68.4°	8.6	0.37
110Ei-m2	110.6	59.0°	7.7	0.41
110Ei-m3	110.6	49.2°	6.8	0.46
110Ei-m4	110.6	39.3°	5.9	0.53
56Ei-m1	56.2	68.4°	6.1	0.52
56Ei-m2	56.2	59.0°	5.5	0.58
56Ei-m3	56.2	49.2°	4.8	0.65
56Ei-m4	56.2	39.3°	4.2	0.76

Table 1: Analysis conditions. The symbol E_i represents the incident energy, $2\theta_{max}$ the largest horizontal scattering angle, Q_{max} the largest momentum transfer for elastic scattering, and the r-resolution, defined as $\Delta r = \pi/Q_{max}$, is denoted as Δr.

2. Experimental setup and data analysis

The INS measurements were performed using the Fermi chopper spectrometer 4SEASONS [12] at the Materials and Life Science Experimental Facility in J-PARC.

The incident energy in a chopper spectrometer can be arbitrarily set by tuning the phase delay of the monochromating chopper, which typically has a rotational frequency (several hundred Hz) that is much higher than the frequency of the pulsed neutron source (25 Hz in J-PARC). Thus, the chopper window opens multiple times within the source period. Accordingly, neutrons of multiple incident energies can pass through a monochromating chopper. We have succeeded in experimentally demonstrating that simultaneous INS measurements using multiple values of E_i can be realized [13]. This method has been referred to as multi-E_i measurement and it has rapidly become widespread as a standard method of INS measurement at pulsed neutron facilities worldwide.

The n-th incident wavelength $\lambda_i(n)$ [Å] selected by a Fermi chopper with the frequency of f [Hz] is given by

$$\lambda_\mathrm{i}(n) = \lambda_\mathrm{i}(1) + \frac{3956 \cdot (n-1)}{2f \cdot L_\mathrm{mc}}, \qquad (1)$$

where $\lambda_\mathrm{i}(1)$ [Å] is the shortest wavelength of the multiple incident neutrons and L_mc [m] the distance between the neutron source and the Fermi chopper. The factor 2 in the denominator of Eq. (1) stems from the fact that a neutron can pass through the Fermi chopper from both sides of the chopper window. The n-th incident neutron energy $E_\mathrm{i}(n)$ [meV] is calculated as

$$E_\mathrm{i}(n) = \frac{81.81}{\lambda_\mathrm{i}(n)^2}. \qquad (2)$$

The phase delay of the Fermi chopper was tuned to select the incident energy of 110.6 meV and set the chopper frequency to 350 Hz. In this condition, other values of E_i can also be selected, i.e., E_i can also take the value of 310.1 meV, 56.2 meV, 33.9 meV, 22.7 meV, and 16.2 meV. In this study we analyzed INS data with E_i = 110.6 meV and E_i = 56.2 meV, where the energy resolutions for elastic scattering equaled 6.6 meV and 2.8 meV, respectively. Approximately 100 g of the polycrystalline Ni powder was sealed in an aluminum can and the measurement was carried out at room temperature for 10 hours at the beam power of 292 kW. The data reduction process performed to produce $S(Q, E)$ was completed using the Utsusemi suite [14], and the conversion from $S(Q, E)$ to $G(r, E)$ was executed using our in-house code written in the Igor Pro programming language.

3. Results and discussion

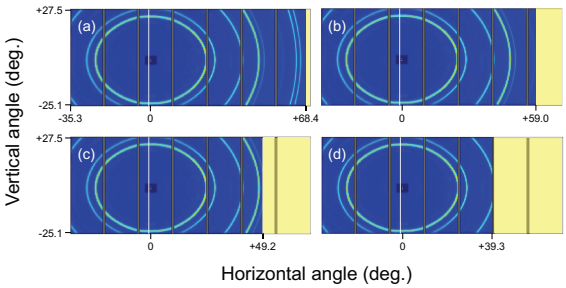

Figure 1: Two-dimensional maps of the intensity distribution from polycrystalline Ni on the detectors. The incident neutron energy in all cases is 110.6 meV. The yellow regions of the maps correspond to the masked detector region. The largest horizontal scattering angle, $2\theta_{max}$, equals (a) 68.4°, (b) 59.0°, (c) 49.2°, and (d) 39.3°.

The detectors of 4SEASONS are ^{3}He position-sensitive with ϕ19 mm × 2500 mm, and they are cylindrically placed at a distance of 2500 mm from the sample. The horizontal scattering angle coverage was from

−35.3° to +68.4°, and the vertical one was from −25.1° to +27.5°. To obtain $S(Q, E)$ by a data reduction process, the data from the defective detectors and pixels can be discriminated using the so-called mask file.

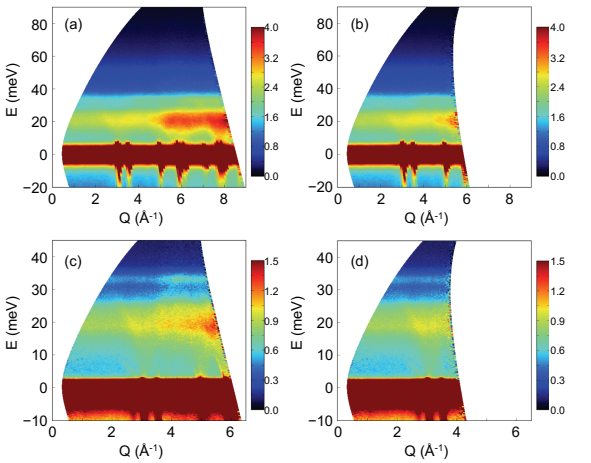

Figure 2: Dynamical structure factor $S(Q, E)$ of polycrystalline Ni. The analysis conditions are (a) 110Ei-m1, (b) 110Ei-m4, (c) 56Ei-m1, and (d) 56Ei-m4, as described in Table 1.

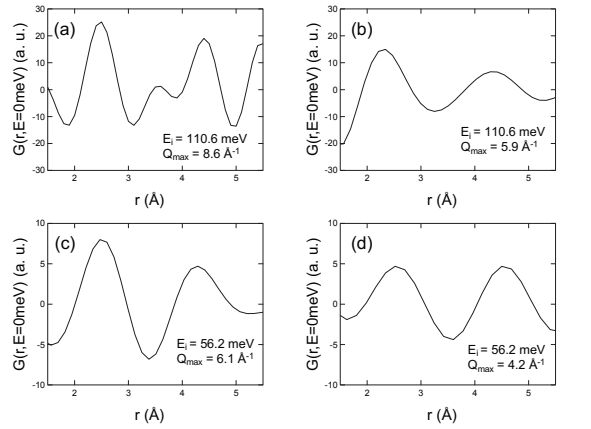

Figure 3: The r-dependences for $G(r, E)$ in the elastic region transformed from the $S(Q, E)$ shown in Fig. 2. The analysis conditions are (a) 110Ei-m1, (b) 110Ei-m4, (c) 56Ei-m1, and (d) 56Ei-m4, as described in Table 1.

To survey the effects of differing Q-E ranges of $S(Q, E)$ on the $G(r, E)$ features, we prepared several different mask files and produced several $S(Q, E)$ data sets. The INS intensity distributions on detectors for polycrystalline Ni with E_i = 110.6 meV are shown in Fig. 1. These intensities were accumulated in the energy transfer range between −20 meV and +100 meV. The detector maps shown in Fig. 1 are analyzed by four types of mask files, and the yellow color denotes the masked detector regions. The largest horizontal scattering angles $2\theta_{max}$ are also indicated. In this paper, the analysis conditions represented by Fig. 1(a)-(d) are referred to as (a) 110Ei-m1, (b) 110Ei-m2, (c) 110Ei-m3, and (d) 110Ei-m4. The details of the analysis conditions for all data sets are listed in Table 1, including the data of E_i = 56.2 meV. The largest momentum transfer values for an elastic scattering Q_{max} are summarized in Table 1, together with the r-resolutions $\Delta r = \pi/Q_{max}$. Note that all analyses listed in Table 1 were performed using one raw data set obtained by one INS measurement.

The two-dimensional $S(Q, E)$ maps of polycrystalline Ni are shown in Fig. 2 for the analysis conditions (a) 110Ei-m1, (b) 110Ei-m4, (c) 56Ei-m1, and (d) 56Ei-m4, as described in Table 1. The strong intensities found around 20 meV and 35 meV are ascribed to the transverse and longitudinal acoustic phonon energies at the zone boundary, respectively.

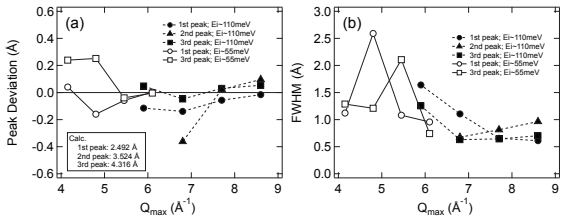

Figure 4: The Q_{max} dependences of the (a) peak deviations from the calculated NN distances, and (b) full width at half maximum (FWHM) of a series of fitted Gaussian peaks.

The r-dependences of $G(r, E)$ in elastic region are given in Fig. 3. For Fig. 3(a)-(b), the integration range equals −5 meV ≤ E ≤ +5 meV, whereas the one for Fig. 3(c)-(d) equals −2 meV ≤ E ≤ +2 meV. The first, second, and third NN distances of Ni are calculated to be 2.49 Å, 3.52 Å, and 4.32 Å, respectively. As shown in Fig. 3(a), $G(r, E)$ for the 110Ei-m1 condition can correctly describe the peaks up to at least the third NN distance. The deviations of the observed peak positions from the calculated NN distances are plotted in Fig. 4(a) for each NN distance, as a function of Q_{max}. Each peak was fitted using a Gaussian function and a linear baseline, and the peak position was assumed to correspond to the center of a fitted Gaussian function. The Q_{max} dependences of the full width at half maximum (FWHM) of a series of fitted Gaussian peaks are shown in Fig. 4(b). The first NN can be correctly evaluated by the $G(r, E)$ transformed from $S(Q, E)$ with Q_{max} being

equal to at least 6 Å, whereas worse r-resolutions make it more difficult to distinguish the second NN peak.

Next, we will discuss the characteristic features of $G(r, E)$ in the inelastic scattering region. In the case of E_i = 110.6 meV, the tail of the elastic scattering was non-negligible up to 20 meV, so we use the data of E_i = 56.2 meV to discuss the acoustic phonon features of polycrystalline Ni. The inelastic $G(r, E)$ under the condition 56Ei-m1 is shown in Fig. 5(a) and the constant r slice of $G(r, E)$ at r = 2.5 Å is presented in Fig. 5(b), where the integration width equaled 0.2 Å. The peak position at $r \approx 2.5$ Å experienced almost no change up to 22 meV, and the energy dependence shown in Fig. 5(b) is found to be in complete agreement with the previously published results ([0.5, 0.5, 0] in Fig. 5 of Ref. [2]). The positive values below an energy of 22 meV occur due to the in-phase atomic correlations, and the negative peak at 33 meV indicates the out-of-phase atomic correlations of longitudinal acoustic phonon at the zone boundary. Therefore, we may conclude that the $G(r, E)$ of polycrystalline Ni under the condition 56Ei-m1 can provide reasonable information on the atomic pair correlations around the first NN.

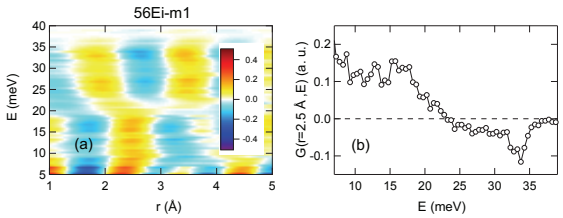

Figure 5: (a) Inelastic $G(r, E)$ of polycrystalline Ni under the condition 56Ei-m1, (b) constant r slice of $G(r, E)$ at $r \approx 2.5$ Å.

It is also important to examine how the smaller Q_{max} affects the inelastic $G(r, E)$ features, which are shown for the conditions 56Ei-m3 and 56Ei-m4 in Fig. 6(a) and Fig. 6(b), respectively. As can be seen in the figure, the peak profiles broaden with a decreasing Q_{max}. The constant E slices at 10 meV $\leq E \leq$ 15 meV are presented in Fig. 6(c), and those at 30 meV $\leq E \leq$ 35 meV in Fig. 6(d). In the low-energy region up to approximately 15 meV, the differences in Q_{max} do not have a large influence on the peak profiles, but they greatly affect the peak profile in the high-energy region around 30 meV.

4. Conclusion

This study presented an investigation of the dynamical structure factor in real-space $G(r, E)$ for polycrystalline Ni, in conjunction with its applicability and limitations. Following the conclusions of previously published studies [10] and those presented in this one, we can be fairly certain that the atomic pair correlations at the first NN distance can be reasonably evaluated using the conventional $S(Q, E)$ with $Q_{max} \approx 6$ Å. These results suggest that many previously accumulated $S(Q, E)$ data sets can be effectively reused for further studies. We are now exploring the possibilities of $G(r, E)$ analysis using the previously measured $S(Q, E)$ data sets.

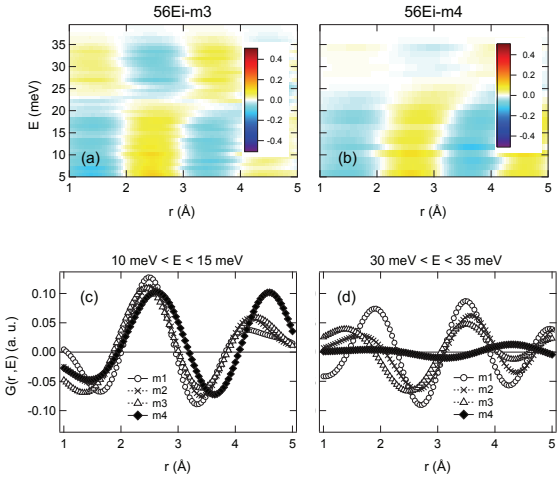

Figure 6: Inelastic $G(r, E)$ of the polycrystalline Ni under the condition (a) 56Ei-m3 and (b) 56Ei-m4. The r-dependence of $G(r, E)$ in the energy range of (c) 10 meV $\leq E \leq$ 15 meV and (d) 30 meV $\leq E \leq$ 35 meV.

To conduct this study, we prepared a large sample (approximately 100 g) and performed a long measurement (approximately 10 hours), but we confirmed that $G(r, E)$ equivalent to that presented in our study can be obtained with a measurement time of 4 hours and a sample amount of approximately 15 g. The required measurement time and sample amount will be drastically reduced when the beam power of J-PARC achieves its expected maximum (1 MW). Furthermore, the horizontal scattering angle of 4SEASONS is planned to have expanded to +127° by January 2019, which means that the research activities in materials science utilizing $G(r, E)$ analysis are expected to accelerate in the near future.

Acknowledgments

The authors gratefully acknowledge S. Shamoto for the permission to use the INS data of polycrystalline Ni and the instrument group staff of 4SEASONS for help with the measurements. The experiments on

4SEASONS were performed under the user program 2014P0901 and 2014A0098.

References

[1] J.M. Carpenter and C.A. Pelizzari, Phys. Rev. B 12 (1975) 2397.

[2] R.J. McQueeney, Phys. Rev. B 57 (1998) 10560.

[3] A.C. Hannon, M. Arai, R.G. Delaplane, Nucl. Instrum. Methods Phys. Res. Sect. A 354 (1995) 96.

[4] A.C. Hannon, M. Arai, R.N. Sinclair, A.C. Wright, J. Non-Cryst. Solids 150 (1992) 239.

[5] M. Arai, A.C. Hannon, T. Otomo, A. Hiramatsu, T. Nishijima, J. Non-Cryst. Solids 192&193 (1995) 230.

[6] W. Dmowski, S.B. Vakhrushev, I.-K. Jeong, M.P. Hehlen, F. Trouw, T. Egami, Phys. Rev. Lett. 100 (2008) 137602.

[7] K. Park, J.W. Taylor, D. Louca, J. Supercond. Nov. Magn. 27 (2014) 1927.

[8] A. Pramanick, W. Dmowski, T. Egami, A. Setiadi Budisuharto, F. Weyland, N. Novak, A.D. Christianson, J.M. Borreguero, D.L. Abernathy, M.R.V. Jørgensen, Phys. Rev. Lett. 120 (2018) 207603.

[9] W. Dmowski, S.O. Diallo, K. Lokshin, G. Ehlers, G. Ferré, J. Boronat, T. Egami, Nat. Commun. 8 (2017) 15294.

[10] M. Nakamura, T. Kikuchi, K. Kamazawa, Y. Kawakita, Phys. B Condens. Matter 551 (2018) 351.

[11] Y. Kawakita, T. Kikuchi, Y. Inamura, S. Tahara, K. Maruyama, T. Hanashima, M. Nakamura, R. Kiyanagi, Y. Yamauchi, K. Chiba, S. Ohira-Kawamura, Y. Sakaguchi, H. Shimakura, R. Takahashi, K. Nakajima, Phys. B Condens. Matter 551 (2018) 291.

[12] R. Kajimoto, M. Nakamura, Y. Inamura, F. Mizuno, K. Nakajima, S. Ohira-Kawamura, T. Yokoo, T. Nakatani, R. Maruyama, K. Soyama, K. Shibata, K. Suzuya, S. Sato, K. Aizawa, M. Arai, S. Wakimoto, M. Ishikado, S. Shamoto, M. Fujita, H. Hiraka, K. Ohoyama, K. Yamada, C.H. Lee, J. Phys. Soc. Jpn. 80 (2011) SB025.

[13] M. Nakamura, R. Kajimoto, Y. Inamura, F. Mizuno, M. Fujita, T. Yokoo, M. Arai, J. Phys. Soc. Jpn. 78 (2009) 093002.

[14] Y. Inamura, T. Nakatani, J. Suzuki, T. Otomo, J. Phys. Soc. Jpn. 82 (2013) SA031.